Warm Period Growth of Travertine during the Last Interglaciation in Southern Germany

Norbert Frank

Heidelberger Akademie der Wissenschaften, Forschungsstelle Radiometrie, Im Neuenheimer Feld 229, D-69120 Heidelberg, Germany

Margarethe Braum

Heidelberger Akademie der Wissenschaffen, Forschungsstelle Radiometrie, Im Nenenheimer Feld 229, D-69120 Heidelberg, Germany

Ulrich Hambach

Geologisches Institut der Universität zu Köln, Zülpicher Strasse 49a, D-50674, Cologne, Germany

Augusto Mangini

Heidelberger Akademie der Wissenschaften, Forschungsstelle Radiometrie, Im Neuenheimer Feld 229, D-69120 Heidelberg, Germany

and

Günther Wagner

Heidelberger Akademie der Wissenschaften, Forschungsstelle Archäometrie, Sanpfercheckweg 1, D-69126 Heidelberg, Germany

E-mail: Norbert.Frank@iup.uni-heidelberg.de

Late-Quaternary travertine at two sites near Stuttgart formed entirely during interglacial periods. The travertine contains structures from growth induced by bacteria, and such structures have been dated by ^{230}Th/U mass spectrometry. The resulting ages from both sites imply growth episodes of short duration, with growth rates up to 5 mm yr^{-1}, at 99,800 ± 1300 yr B.P. (2σ; $n = 8$) and 105,900 ± 1300 yr B.P. (2σ; $n = 7$). These episodes were likely part of marine isotope stage (MIS) 5.3. Deposition of silt interrupted travertine growth at one of the sites ~105,000 yr B.P. Likely correlatives of this silt are the St. Germain I-B stade recorded in the Grand Pile peat bog and a cold episode ~1000 yr long recorded by δ^{18}O values in the GRIP ice core. Travertine also formed during stage 5.5 (~115,000 yr) and during the early Holocene. We found no evidence for travertine accumulation in stages 2, 3, 4, and 5.1. At both sites, the Sr/U ratio and the initial ^{234}U/^{238}U activity ratio resemble those of modern spring water. However, the sites differ in the chemical composition of spring water and in stratigraphic sequence of travertine accumulation.   © 2000 University of Washington.

Key Words: travertine; thermal ionization mass spectrometry; thorium/uranium dating; Quaternary climate; central Europe.

INTRODUCTION

The growth of secondary carbonates has potential as a measure of climatic change (Harmon *et al.,* 1979; Roberts *et al.,* 1998; Taylor *et al.,* 1994; Baker *et al.,* 1993; Goudie *et al.,* 1993). We investigated travertine and calcareous tufa from Stuttgart-Bad Cannstatt, Germany (Fig. 1).

Travertine and tufa commonly originate from physicochemical and microbiological carbonate deposition from thermal groundwater containing elevated carbon dioxide concentrations (Ford and Pedley, 1996; Pedley, 1994; Pentecost, 1996). Because carbonate precipitation occurs in contact with the atmosphere and biosphere of the spring area, pollen records of travertine may be linked to other climate archives, such as peat deposits. Furthermore, thermal spring deposits characterized by high accumulation rates (>1 mm yr^{-1}) can be used for high-resolution studies of climatic variability.

Near Stuttgart, travertine and tufa may record growth episodes within each interglaciation during the past 500,000 years (Reiff, 1986). The climatic signal recorded by the travertine is the simplest possible, because travertine growth probably ceased during glaciations due to permafrost. Thus,
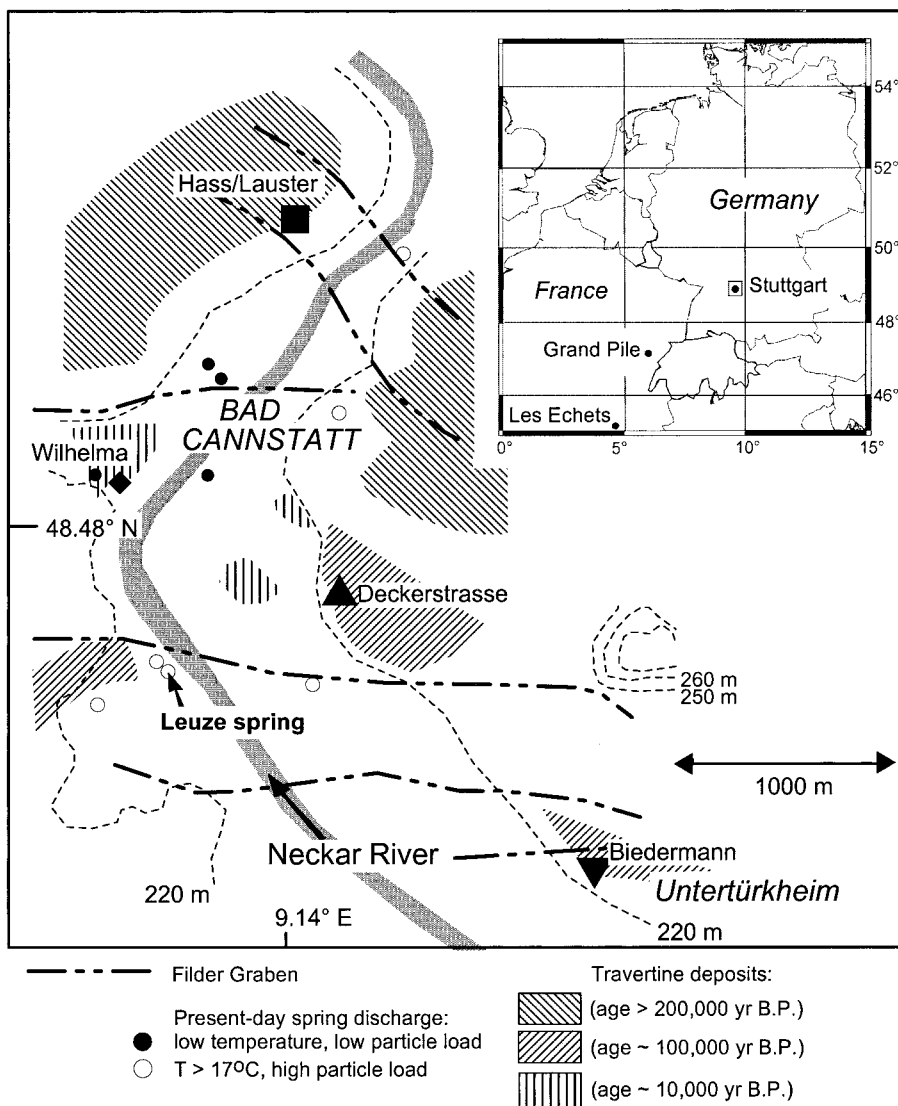
FIG. 1. Location of the travertine deposits in Bad Cannstatt. The deposits formed near the Neckar valley in various areas (shaded), close to modern spring water sources (solid and open circles). Triangles mark the sampling sites at Deckerstrasse and Biedermann.

given a continuous growth record and negligible erosion, dating growth episodes at Stuttgart could improve the glacial/interglacial chronology of central Europe.

With mass spectrometric [230]Th/U techniques and isochron methods, travertine can be dated accurately from 1000 to 500,000 yr B.P. (Ludwig *et al.,* 1992; Sturchio *et al.,* 1994; McDermott *et al.,* 1993; Lin *et al.,* 1996). The accuracy of [230]Th/U chronologies of carbonates requires closed-system behavior and negligible or even [232]Th-correctable abundance of [230]Th, [234]U, and [238]U from detritus (Kaufman and Broecker, 1965; Kaufman, 1992; Lin *et al.,* 1996; Ludwig and Titterington, 1994). In this study we combine mass spectrometric uranium series measurements of specific bacterial-induced carbonate samples and modern groundwater with geochemical records to verify the dating presumptions and to characterize the material and locations.

GEOLOGIC SETTING AND SAMPLE LOCATION

Bad Cannstatt travertine deposits have grown from groundwater that rises at the Filder Graben (Reiff, 1986) (Fig. 1), and they extend over several km[2]. The thermal groundwater system is one of the most important mineral water systems of central Europe, with outflow rates of 500 liter s[-1] (Uffrecht, 1994). The water is highly mineralized and has Ca concentrations of up to 560 mg liter[-1]. All travertines exhibit similar lithologic sequences. Prior to carbonate formation, glacial terrace gravel and lake sediments were deposited. In the following intergla-

ciation the growth of secondary carbonates typically started in a lake environment, characterized by calcareous tufa deposits with plant encrustations (Koban, 1993; Reiff, 1986). Here the carbonate was precipitated as characeen-ostracode tufa (later referred to as reed-encrusted tufa) (Koban, 1993). When the shallow lake was filled with carbonate, plant growth ceased and formation of laminar dense travertine of various types began. Peloidal structures, like gas bubble layers of cyanobacterial origin and bacterial stromatoliths, dominate in last-interglacial deposits as well as in Holocene travertines, whereas the older deposits often contain significant amounts of phytoherm framework and laminar shrubs (Koban, 1993). During colder periods, travertine growth ceased due to reduced recharge and permafrost (Reiff, 1986). Eventually the travertine deposits were covered by loess. The travertine deposits formed almost as horizontally as river terraces; thus, all sites should have a simple relationship between travertine height and age.

We collected samples at travertine quarries at Deckerstrasse in the center of Bad Cannstatt and at the Biedermann site in Untertürkheim (Fig. 1). Both deposits originate at a similar altitude in the Neckar valley; the gravel beneath the travertine is of similar thickness, indicating that both deposits accumulated during the same interglaciation (Reiff, 1986). However, the lithological sequence differs at each sites. The Deckerstrasse travertine is only 2.5–3 m thick. Its basal unit is 20–50 cm of reed-encrusted tufa that grew on top of ~2-m-thick mud layers of an ancient lake. Above the reed-encrusted tufa, 2.2–2.5 m of laminar travertine accumulated without growth interruptions. Travertine-sand layers and small stalagmites in larger cracks give evidence of weathering and erosion. In contrast, the Biedermann travertine exhibits a far more complex growth structure up to 8.5 m thick with many textural changes and one silt layer interrupting the travertine growth. The silt layer, 20 cm thick, represents a cold, dry period when travertine accumulation did not take place, but it does not reflect a glaciation (Reiff, 1986).

Schweigert (1991) studied the floral record at this site. He concluded that the occurrence of a Mediterranean honeysuckle tree (*Lonicera arborea boissier*) indicates a climate of less-continental character. The forest around the former springs was dominated by oak (*Quercus*) and ash (*Fraxinus*), comparable to either the Eemian or the St. Germain I (St. Geneys 1) stage recorded in the pollen spectra of the Grand Pile peat bog (Woillard, 1976; Guiot *et al.,* 1989) and at Les Echets (Reille and de Beaulieu, 1990).

Various studies were previously undertaken to determine the age of these supposedly last-interglacial travertines. Grün *et al.* (1982), M. Geyh (personal communication), and Braun *et al.* (1998) determined radiometric ^{230}Th/U ages of the Biedermann and Deckerstrasse sites and related travertine deposits of similar geological setting, yielding average ages of 109,000 $\pm$ 25,000 (2σ ($n = 6$), 124,000 $\pm$ 40,000 (2σ) ($n = 15$), and 124,000 $\pm$ 12,000 (2σ) ($n = 44$) yr. The results reported by Braun *et al.* (1998) clearly demonstrate a cluster of ages at 109,000 $\pm$ 10,000 yr ($n = 22$) for the Deckerstrasse site. However, extremely high ages of up to 200,000 yr were reported, which reflect uranium mobilization within the travertine. In summary, all studies carried out thus far indicate that travertine accumulation took place about 100,000–125,000 yr B.P.—during a full interglaciation corresponding to isotope stage 5 (Martinson *et al.,* 1987). Grün *et al.* (1982) further inferred that the silt layer at the Biedermann site represents the transition from stage 5.5 to stage 5.4 corresponding to the Melisey I Stade determined at Grand Pile. However, these earlier interpretations are based on low-precision ages.

Using a portable drilling device with a diamond blade, cores 50 mm in diameter and 360 mm long were taken at both sites in a way that covered the vertical and horizontal extent of the travertine outcrops. In addition, we analyzed the water of the "Leuze" spring, which has an intermediate chemical composition compared to all other modern springs of the studied area (Uffrecht, 1994).

SAMPLE PREPARATION

Travertine cores were rinsed twice with distilled water (60°C) and 0.1 N HNO_3 to remove surface contamination. The cores were subdivided into different microbiological structures (Table 1, Fig. 2). These splits were precleaned with heated distilled water, nitric acid, and ultrasound.

The samples were crushed and sieved to a size fraction of 125–250 μm to minimize the influence of detritus. This size fraction was again precleaned twice. Samples 0.3 to 1 g in weight were then dried, weighed, and dissolved in concentrated suprapure nitric acid. To determine the uranium and thorium concentrations, defined quantities of a ^{233}U/^{236}U spike (^{233}U/^{236}U atomic ratio of 0.8579 $\pm$ 0.0025) and a ^{229}Th spike were added. Before chemical separation, the insoluble silicate components of the travertine samples were centrifuged, dried, and weighed to determine the average contamination with detritus. Sample aliquots were taken for Sr, Mg, Mn, and Fe measurements using atomic absorption spectrometry (AAS).

Chemical separation and purification of uranium and thorium closely followed the procedure described by Ivanovich and Harmon (1992). Thorium and uranium isotopes were separated using iron for coprecipitation, purified utilizing DOWEX 1 × 8 resin in nitric form, and placed on a preheated rhenium filament for mass spectrometric analyses. Chemical blanks yielded less than 0.2 ng ^{238}U and 0.13 ng ^{232}Th, respectively.

MASS SPECTROMETRY

Thorium and uranium measurements were made on a multicollector mass spectrometer (Finnigan MAT 262 RPQ) with

TABLE 1
Thorium and Uranium Activities and Activity Ratios of Travertine Samples from the Biedermann and Deckerstrasse Sites

	Height (m)	Sample/ code[d]	^{230}Th[a] (dpm/g)	^{232}Th[a] (ppm)	^{234}U[a] (dpm/g)	^{238}U[a] (ppm)	$(^{234}U/^{238}U)_m$	$(^{234}U/^{238}U)_i$[c]	$(^{230}Th/^{234}U)$	$(^{230}Th/^{232}Th)$	Age[b] (10^3 yr)	Residue (%)
BN6	7.5	cs, ps	0.2149 ± 0.0044	0.0566	0.3286 ± 0.0007	0.2309	1.903 ± 0.004	2.187 ± 0.033	0.6540 ± 0.014	15.5	96.7 ± 9.6	n.d.
BN4	6.7	lt, pf	n.d.		0.5129 ± 0.0072	0.3550	1.932 ± 0.027					
Bi7+	6.5	gbl, ps	0.3382 ± 0.0025	0.043	0.5114 ± 0.0027	0.3567	1.917 ± 0.010	2.238 ± 0.016	0.6614 ± 0.006	320.8	105.6 ± 2.4	1.67
Bi1	5.9	lt, pf	0.3323 ± 0.0047	0.0179	0.4930 ± 0.0026	0.3423	1.926 ± 0.010	2.256 ± 0.022	0.6741 ± 0.010	75.8	107.5 ± 4.8	1.43
BN5	5	lt, pf	0.2833 ± 0.0023	0.0147	0.4250 ± 0.0032	0.2915	1.950 ± 0.015	2.281 ± 0.023	0.6665 ± 0.007	79.0	105.5 ± 3.5	n.d.
Bi2	4.75	gbl, ps	0.2934 ± 0.0064	0.0065	0.4528 ± 0.0014	0.3170	1.910 ± 0.006	2.216 ± 0.021	0.6481 ± 0.014	183.8	102.2 ± 5.7	1.02
Bi3	4.2	gbl, ps	0.2988 ± 0.0031	0.0056	0.4517 ± 0.0050	0.3116	1.939 ± 0.021	2.265 ± 0.032	0.6615 ± 0.010	219.9	105.4 ± 4.0	1.21
Bi4	2.95	gbl, ps	0.2537 ± 0.0074	0.0233	0.3782 ± 0.0020	0.2611	1.937 ± 0.010	2.264 ± 0.035	0.6706 ± 0.020	44.5	105.6 ± 9.0	1.78
Bi5*	2.85	lt, pf	0.2894 ± 0.0023	0.0918	0.4152 ± 0.0063	0.2877	1.930 ± 0.029	2.251 ± 0.050	0.6971 ± 0.012	12.9	104.6 ± 8.8	4.58
Bi8	2.15	gbl, ps	0.2578 ± 0.033	0.0357	0.3780 ± 0.0019	0.2650	1.908 ± 0.010	2.229 ± 0.025	0.6819 ± 0.009	29.5	106.8 ± 6.0	2.82
BN3	0.6	rec, cot	0.3162 ± 0.0024	0.2575	0.4405 ± 0.0022	0.3060	1.925 ± 0.010	2.206 ± 0.063	0.7177 ± 0.007	5.0	93.6 ± 18.2	n.d.
Bi9	0.35	rec, cot	0.2730 ± 0.0049	0.0353	0.3748 ± 0.0021	0.2453	2.043 ± 0.011	2.458 ± 0.035	0.7284 ± 0.014	31.6	118.3 ± 7.7	1.92
BN1	0.3	rec, cot	0.2718 ± 0.0083	0.0163	0.3944 ± 0.0029	0.2707	1.948 ± 0.014	2.299 ± 0.039	0.6892 ± 0.022	68.2	111.2 ± 9.2	n.d.
De1/1+	2.6	gbl, ps	0.1516 ± 0.0017	0.0086	0.2367 ± 0.0022	0.1525	2.076 ± 0.021	2.424 ± 0.032	0.6404 ± 0.009	71.6	98.6 ± 4.1	1.67
De2*	1.3	gbl, ps	0.1851 ± 0.0032	0.0238	0.2594 ± 0.0025	0.1719	2.018 ± 0.021	2.408 ± 0.040	0.7137 ± 0.014	31.7	114.5 ± 6.7	4.58
De2/4	1.22	ps, (1)	0.1486 ± 0.0033	0.0025	0.2357 ± 0.0025	0.1549	2.035 ± 0.031	2.365 ± 0.046	0.6304 ± 0.015	246.5	97.7 ± 5.9	1.78
De2/3	1.21	gbl, ps	0.1645 ± 0.0022	0.0031	0.2481 ± 0.0021	0.1626	2.040 ± 0.018	2.402 ± 0.029	0.6633 ± 0.010	214.1	105.3 ± 4.2	1.21
De2/2	1.2	gbl, ps	0.1435 ± 0.0019	0.0024	0.2210 ± 0.0019	0.1433	2.062 ± 0.023	2.418 ± 0.036	0.6493 ± 0.010	242.6	101.9 ± 4.7	1.02
De2/1	1.19	ps, (2)	0.1620 ± 0.0023	0.0040	0.2496 ± 0.0029	0.1672	1.996 ± 0.025	2.330 ± 0.038	0.6488 ± 0.012	165.4	101.9 ± 4.7	1.43
De7	0.7	gbl, ps	0.1865 ± 0.0024	0.0167	0.2736 ± 0.0025	0.1915	1.910 ± 0.018	2.238 ± 0.031	0.6818 ± 0.011	45.5	108.4 ± 5.5	2.82
De3/1	0.2	rec, cot	0.1647 ± 0.0068	0.0013	0.2345 ± 0.0015	0.1605	1.955 ± 0.018	2.328 ± 0.050	0.7021 ± 0.029	510.9	116.4 ± 11.4	1.92
De5/1	0	rec, cot	0.1028 ± 0.0033	0.0005	0.1478 ± 0.0019	0.0982	2.013 ± 0.033	2.401 ± 0.058	0.6956 ± 0.024	844.9	114.3 ± 9.3	n.d.

Note. (*) Samples with large amounts of detritus; (+) contaminated by Fe-hydroxide in pores; (n.d.) not determined.

[a] Uncertainties of ^{230}Th and ^{234}U are given as 2σ absolute values of concentration measurements, including reproducibility determined with NBL 112a and thorium standard material. Uncertainties of ^{238}U and ^{232}Th measurements are typically on the order of ±0.5% (2σ).

[b] Model ages are iteratively determined from ^{232}Th corrected activity ratios (Eq. (A1) in Appendix), applying Eq. (1) (Ivanovich and Harmon, 1992).

$$\frac{^{230}Th}{^{234}U} = \frac{^{238}U}{^{234}U} \cdot (1 - e^{-\lambda_{230} \cdot t}) + \frac{\lambda_{230}}{\lambda_{230} - \lambda_{234}} \left(1 - \frac{^{238}U}{^{234}U}\right) \cdot (1 - e^{-(\lambda_{230} - \lambda_{234}) \cdot t}). \tag{1}$$

Here, λ_{230} ($= 9.195 \times 10^{-6}$) and λ_{234} ($= 2.835 \times 10^{-6}$) are the decay constants following Edwards *et al.* (1987).

[c] Equation (2) was applied to estimate initial ^{234}U/^{238}U activity ratios (see text).

$$\left(\frac{^{234}U}{^{238}U}\right) = \left(\left(\frac{^{234}U}{^{238}U}\right)_0 - 1\right) e^{\lambda_{234} \cdot t} + 1. \tag{2}$$

[d] Sample descriptions: gbl, ps, gas bubble layers, peloidale structures; pl, peloidale layers; lt, leaf tufa; cs, carbonate sand; rec, reed-encrusted; cot, characeen-ostracode tufa; ls, laminar shrubs; pf, phytoherm framework.

a double filament technique. Measurements of uranium were carried out with thermal fractionation values of less than 0.2% per mass unit (determined with the ^{233}U/^{236}U internal reference and adopting the natural ^{238}U/^{235}U atomic ratio of 137.88). Uranium standard material NBL (former National Brunswick Laboratories) 112a, measured before and after four or fewer samples, yielded an average ^{234}U/^{238}U atomic ratio of 52.62 × 10^{-6} ± 1.9‰ (2σ mean) (Table 2) (^{234}U = (^{234}U/^{238}U$_{measured}$/^{234}U/^{238}U$_{equilibrium}$ − 1) · 1000 = −38.5 ± 2.4‰), in good agreement with the value given by Chen *et al.* (1986) and Bard *et al.* (1996), and ~2‰ lower than one reported by Edwards *et al.* (1993). Previous measurements at our facility reported by Eisenhauer *et al.* (1996), Bollhöfer *et al.* (1996), and Burns *et al.* (1998) are 4‰ higher because we did not consider the abundance sensitivity as a significant contribution (up to +3‰). In these earlier measurements we did not perform

continued calibration of Faraday to ICM efficiency, measuring mass 235 in both detectors. In the present study we performed this calibration, which yields a more precise thermal fractionation correction. The abundance sensitivity correction follows the assumption that the amount of scatter ions from mass 238, contributing to mass 234, decreases exponentially from mass 237.7 to mass 234.0. The abundance sensitivity was determined with a detailed mass scan before each standard measurement and contributes up to 3‰ to the overall 234 signal.

The external reproducibility of the concentration was determined with sample duplicates and concentration measurements of standard solution prepared with NBL 112a (^{238}U = 4.390 ppm) and yields a value of ±0.5% (2σ). The external reproducibility for thorium is ±0.8% (2σ), determined with a ^{232}Th internal standard. It is approximately 1.5 times less than that for uranium due to the unknown instrumental fractionation.
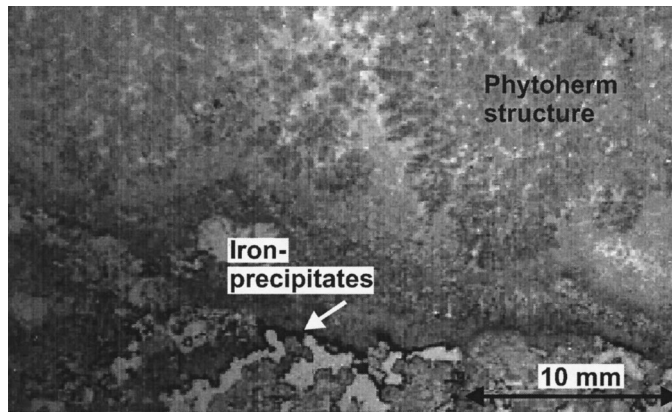
FIG. 2. Thin section of a travertine sample showing deposition of carbonate due to phytoherm activity (upper right and left part). Below the phytoherm structure indicated by the tuft texture, carbonate was precipitated as a laminar band. Below this laminar structure is a gas bubble layer. Ferromanganese precipitates at the bubble surfaces may have been precipitated *in situ* due to the high iron abundance of the spring water (0.05–16 mg liter^{-1}). For uranium series measurements, the phytoherm structure was cut off. In most other cases we sampled abundant gas bubble layers, peloidale layers, or laminar shrubs almost free of ferromanganese coating and pore cement.

AAS ANALYSES

Sr, Mg, Mn, and Fe concentrations were measured on a Varian-SpectrAA.10 atomic absorption spectrometer applying 3-point calibration of appropriate standard solutions. Statistical uncertainties are less than $\pm 10\%$ (2σ) for all elements.

RESULTS

The spring water sample has a ^{238}U-concentration of 1.413 ± 0.012 ppb and a $^{234}U/^{238}U$ activity ratio of 2.114 ± 0.030 (2σ).

Thorium is 750 times less abundant, with a concentration of 1.901 ± 0.011 ppt. The $^{230}Th/^{232}Th$ activity ratio is 1.85 ± 0.71 and the $^{230}Th/^{234}U$ activity ratio is rather small, amounting to 0.0004 ± 0.00012.

Most of the travertine samples consist of low-magnesium calcite with densities of up to 2.5 g cm^{-3} (Tables 1 and 3). Insoluble residues are typically on the order of 1.5%. The average contamination with detrital material is small, yielding ^{232}Th concentrations as low as 0.0005 ppm.

The abundance of manganese, strontium, and magnesium is generally low and comparable at both sites. Concentrations range from 1500 to 2700 ppm Mg, 450 to 840 ppm Sr, and 85 to 240 ppm Mn. In contrast to Mn, Fe shows high abundances >1500 ppm in samples with large amounts of detritus (Table 1) or with contamination by Fe hydroxides in the pore space (Table 1), such as samples Bi5, Bi7, De1/1, and De2.

The U/Sr ratio ranges between 2.0×10^{-4} to 5.1×10^{-4}, a range that includes the U/Sr ratio of 3.0×10^{-4} of modern spring water. A linear trend of the uranium–strontium relationship at each location reflects the chemical composition and physical properties of the water during carbonate precipitation (Fig. 3).

The travertine sites differ clearly in uranium abundance. Highest values of 0.29 to 0.35 ppm occur at the Biedermann site, whereas lowest values down to 0.01 ppm (De5/1) were measured in samples from Deckerstrasse. U, Sr, and Mg content do not vary significantly among the different growth structures. However, cyanobacterial layers and peloidale structures show only small concentrations of ^{232}Th (less than 0.02 ppm) compared with some samples of reed-encrusted tufa, leaf tufa, and carbonate sand.

The $^{230}Th/^{234}U$ and $^{234}U/^{238}U$ activity ratios are quite uniform

TABLE 2
Uranium Standard Measurements Performed with a Mixture of NBL 112a (=NBS-SRM960, NIST-4321B) and $^{233}U/^{236}U$ Double Spike

	$^{234}U/^{238}U \times 10^{-5\ a}_{corr}$	$\delta^{234}U(‰)_{corr}{}^{c}$	$^{233}U/^{236}U{}^{b}$	Detector-combination^{d}
	5.271 ± 0.014	-36.7 ± 2.6	0.8589 ± 0.0038	ICM/F2-F4
	5.270 ± 0.020	-36.9 ± 3.6	0.8564 ± 0.0043	RPQ/F2-F4
	5.279 ± 0.023	-35.3 ± 4.2	0.8544 ± 0.0043	ICM/F2-F4
	5.254 ± 0.030	-39.8 ± 5.5	0.8638 ± 0.0071	ICM/F2-F4
	5.256 ± 0.016	-39.5 ± 2.9	0.8576 ± 0.0030	ICM/F2-F4
	5.240 ± 0.035	-42.4 ± 6.4	0.8555 ± 0.0063	RPQ/F2-F4
	5.267 ± 0.026	-38.9 ± 4.8	0.8586 ± 0.0052	ICM/F2-F4
Average:	5.262 ± 0.010	-38.5 ± 1.8	0.8579 ± 0.0023	

^{a} Given atomic ratios of $^{234}U/^{238}U$ and values of $\delta^{234}U$ are corrected for spike background, thermal fractionation, ICM-Faraday yield drift, and abundance sensitivity. For runs with the first-stage ICM the abundance correction followed an exponential fit through the background spectrum determined from mass 237.7–236.2 and counts on half mass between all other peaks (i.e., 233.5, 234.5, 235.5, and 236.5), yielding average values of 1.6×10^{-7} times ^{238}U on mass ^{234}U (= +3.1‰).

^{b} Atomic ratios of $^{233}U/^{236}U$ represent measured values corrected only for abundance sensitivity. The abundance sensitivity correction is negligible for measurements using the retarding potential quadruple (RPQ) (i.e., less than 0.1‰).

^{c} $\delta^{234}U = (^{234}U/^{238}U_{measured}/^{234}U/^{238}U_{equilibrium} - 1) \cdot 1000)$ applying $^{234}U/^{238}U_{equilibrium} = 5.472 \times 10^{-5}$.

^{d} (ICM) Ion counting electron multiplier; (RPQ) retarding potential quadrupol + electron multiplier; (F) Faraday cup.

TABLE 3
Geochemical Data of Selected Travertine Samples from the Biedermann and Deckerstrasse Sites

	Iron (ppm)	Manganese (ppm)	Magnesium (ppm)	Strontium (ppm)
Bi7	1279 ± 90	143 ± 10	2016 ± 141	840 ± 59
Bi1	1040 ± 73	167 ± 12	2293 ± 160	685 ± 48
Bi2	616 ± 43	72 ± 5	1922 ± 135	747 ± 52
Bi3	511 ± 36	93 ± 7	1964 ± 137	836 ± 59
Bi4	1013 ± 71	85 ± 6	2489 ± 174	621 ± 43
Bi5	1521 ± 106	234 ± 16	2634 ± 184	626 ± 44
Bi8	894 ± 63	121 ± 8	2227 ± 156	618 ± 43
Bi9	836 ± 59	155 ± 11	1986 ± 139	528 ± 37
De1/1	2200 ± 200	130 ± 5	1530 ± 100	830 ± 25
De2/1	730 ± 51	130 ± 9	1665 ± 117	772 ± 54
De2/2	655 ± 46	130 ± 9	1751 ± 123	675 ± 47
De2/3	838 ± 59	133 ± 9	1681 ± 118	693 ± 49
De2/4	1048 ± 73	144 ± 10	1549 ± 108	701 ± 49
De2	1439 ± 101	153 ± 11	2423 ± 170	747 ± 52
De7	815 ± 30	101 ± 5	2129 ± 100	830 ± 30
De3/1	322 ± 9	54 ± 2	1685 ± 33	608 ± 9
De5/1	350 ± 50	95 ± 9	1400 ± 130	450 ± 25

Note. Uncertainties are given as ±5% (1σ) external reproducibility, determined with sample duplicates and reproducibility of 3-point standard calibration.

at each locality. Both deposits exhibit a similar range of ^{230}Th/^{234}U and ^{234}U/^{238}U activity ratios of 0.6–0.7 and 1.91–2.1, respectively. Additionally, the samples of the laminar travertine sequences show a less significant scatter of the ^{230}Th/^{234}U and ^{234}U/^{238}U activity ratios at each site, indicating very fast growth. Especially at Biedermann, the activity ratios are strikingly uniform in part of the laminar travertine. Scatter and high ratios are limited to basal samples where weathering is indicated by small stalagmites in larger cracks and by a red-brownish color of the cement in pores. However, these slightly higher ^{230}Th/^{234}U activity ratios (Table 1; Figs. 4 and 5) may simply indicate a greater age for these layers.

Using ^{232}Th-corrected activity ratios (see the Appendix for correction model), we calculated ^{232}Th-corrected ages for the travertine deposits at the Deckerstrasse and Biedermann sites (Figs. 4 and 5). Because our samples contain only small amounts of detritus, the ^{232}Th-corrected ages differ only by 0.5 to 1.5% from uncorrected values. Ages from laminar travertine samples do not exhibit a significant trend toward higher ages with increasing height of sampling. Thus, we assume that these samples grew cogenetically compared to the age resolution achieved.

Assuming that samples are cogenetic, one obtains a weighted average age for the laminar travertine (0.2–2.5 m at Deckerstrasse; 0.5–6.5 m at Biedermann) of 103,200 ± 3800 yr B.P. at Deckerstrasse and 105,300 ± 1200 yr B.P. at Biedermann, respectively. Age uncertainties are given as 2σ

errors based on 2σ uncertainties of average ^{230}Th/^{234}U and ^{234}U/^{238}U activity ratios.

To check the accuracy of our ages, we calculated the ^{232}Th-free end-member isotope ratios, applying Rosholt Type II isochrons for cogenetic samples (Kaufman, 1992; Ludwig and Titterington, 1994). For the laminar travertine of Deckerstrasse, the ^{232}Th-free endmember isotopic ratios of ^{230}Th/^{234}U and ^{234}U/^{238}U are 0.6377 ± 0.0058 and 2.048 ± 0.012, which yield an age of 99,800 ± 1400 yr B.P. (Figs. 6A and 6B).

Similarly, the application of Rosholt Type II isochrons for cogenetic samples from the laminar travertine at Biedermann yields ^{232}Th-free end-member isotope ratios of ^{230}Th/^{234}U = 0.661 ± 0.006 and ^{234}U/^{238}U = 1.920 ± 0.009 (Figs. 6C and 6D), from which an age of 105,900 ± 1300 yr B.P. is obtained. The good agreement of isochron ages with the simple correction model leads to the conclusion that the initial ^{230}Th/^{232}Th ratio, determined from the spring water sample, is representative for the Biedermann site.

Samples of the reed-encrusted tufa (not included in Fig. 6) are not necessarily the same age as the laminar travertine because weathering and erosion can disguise unconformities between laminar and reed-encrusted travertine. Furthermore, times of nonaccumulation of travertine may not be recorded; the travertine records might be discontinuous. However, field observations and paleomagnetic data (J. Reinders, unpublished data, 1998) show no evidence that the reed-encrusted tufa is older than the laminar travertine.

The reconstructed initial ^{234}U/^{238}U activity ratio for the laminar travertine at Deckerstrasse and Biedermann (Eq. (2), Table 1) yields values of 2.361 ± 0.024 and 2.237 ± 0.016, respectively, significantly different from each other and from present-day spring water (2.114 ± 0.030). This difference is confirmed
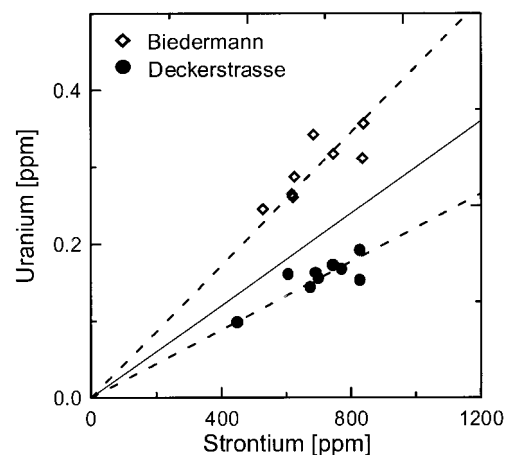

FIG. 3. Correlation of strontium and uranium for the travertine deposits and for modern spring water of intermediate chemical composition. Dashed lines show linear trends for the Biedermann and Deckerstrasse deposits. Solid line shows the Sr/U ratio of present spring water.
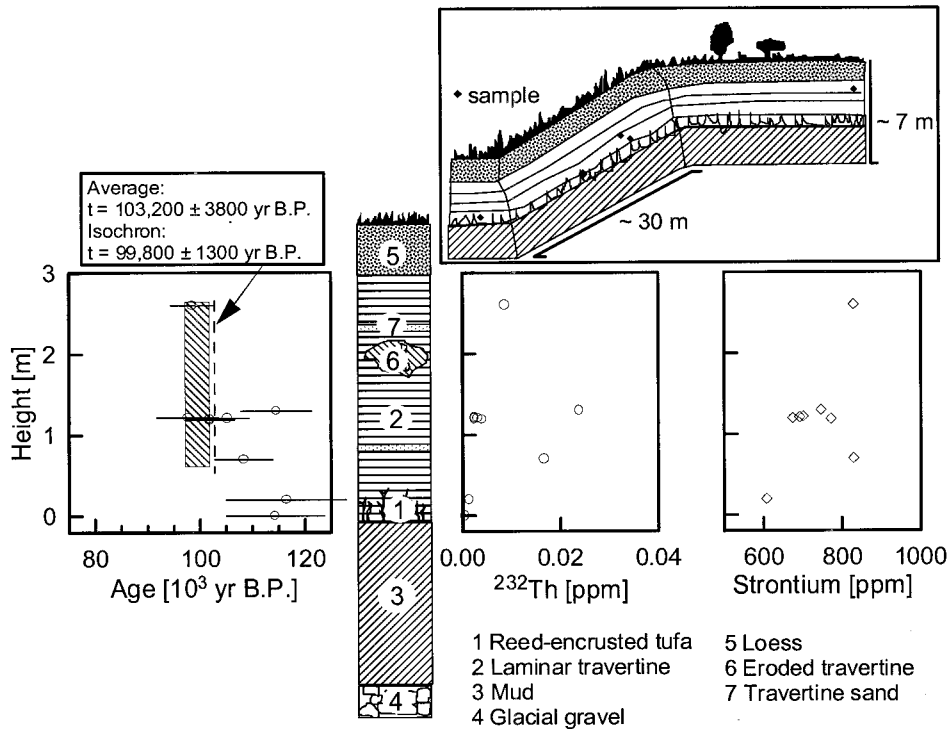
FIG. 4. Travertine sequence at the Deckerstrasse site. In the age graph at left, the ruled area shows the isochron age.

by the deviating U/Sr ratios, also indicating distinct geochemical compositions for the ancient and modern groundwater.

DISCUSSION

Growth of travertine at Biedermann and Deckerstrasse site is restricted to short episodes during interglacial stage 5.3. Here we discuss travertine formation in the context of central European climate chronologies (top of Fig. 7) and global climate cycles (Figs. 7B and 7C).

The travertine formed initially in a lake during a time of transition between interglacial and glacial climates. This conclusion is supported by the floral record determined by Schweigert (1991). He found mainly leaf imprints of reeds but no evidence of ash (*Fraxinus*) or oak (*Quercus*) trees within the bottom part of the travertine at the Biedermann site (0 to 0.9 m height). Ash and oak dominated the floral record in central Europe during interglacial substages 5.5, 5.3, and presumably also 5.1.

As erosion or missing accessibility of the initial travertine deposit may truncate the chronology, we can not determine precisely the time of the earliest growth episode. Our data suggest, however, an age near the end of interglacial substage 5.5, or even the beginning of 5.3. We do not understand yet why the Eemian episode is not strongly represented within the Bad Cannstatt area. Because travertine formation occurred mainly as reed-encrusted tufa during the early Holocene, and not in the middle and late Holocene, the missing evidence of travertine formation during the Eemian episode could reflect climate conditions similar to those of the middle Holocene.

The average age of ~105,000 yr B.P. determined for the fast-growing laminar travertine resembles that of substage 5.3; it is also the estimated age of interstadial episode St. Germain I and St. Geneys I (Guiot *et al.,* 1989). At Biedermann, this part of the sequence (0.9 to 6 m) contains not only leaf imprints of oak and ash but also remains of poplars (*Populus*) and Mediterranean honeysuckle trees (*Lonicera arborea boissier*). These fossils indicate a warm climate. The growth rate of the travertine was extremely high during this episode (up to 5 mm yr^{-1}), for there is no significant trend of ^{230}Th/^{234}U ages.

The growth interruption (silt layer) at the Biedermann site reflects a cold period ~1000 yr long. Radionuclide activity ratios do not differ significantly between samples above and beneath the silt (triangles in Fig. 7a). The floral record of the silt records a decline of the local forest vegetation. We infer that this episode coincides with the cooling event recorded in the δ^{18}O values of the GRIP ice core approximately 105,000–104,000 yr B.P. (Dansgard *et al.,* 1993) (Fig. 7B). A similar cooling event is recorded in the Grand Pile and Les Echets peat bogs, as St. Germain I-B and St. Geneys I-B (Guiot *et al.,* 1989). However, this correlation is weak because peat records are not accurately dated compared to our travertine record and, furthermore, both types of records are probably discontinuous.
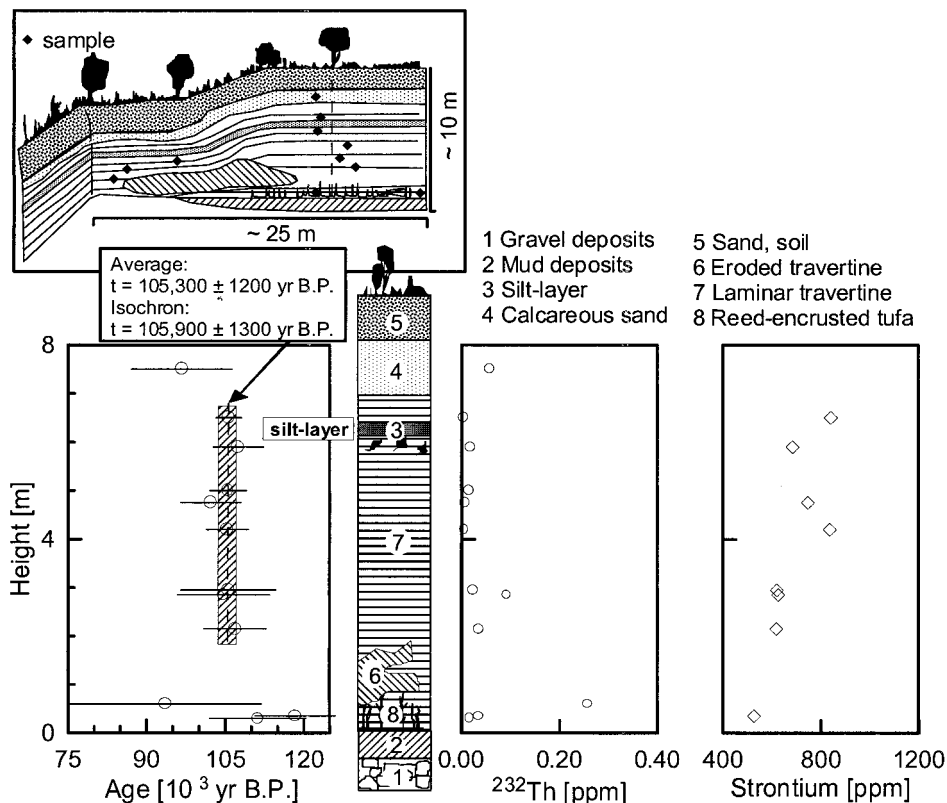
FIG. 5. Travertine sequence at the Biedermann site. At left, the ruled area shows the isochron age.

How does the travertine record at the Deckerstrasse site (diamonds in Fig. 7A) fit into this picture? As mentioned above, both deposits began to grow in a lake environment. At the Deckerstrasse site the mud layer beneath the carbonate formation is 2 m thick, compared to only 0.2–0.5 m at the Biedermann site. This greater thickness implies higher lake levels. The two sites yielded similar ^{230}Th/^{234}U ages for reed-encrusted tufa. However, the groundwater composition was different, as shown by U/Sr and initial ^{234}U/^{238}U activity ratios. The laminar travertine evolved several thousand years later at Deckerstrasse (Rosholt Type II Isochrons age 101,000–98,000 yr) than the Biedermann site, synchronous with the part of the sequence above the silt layer at Biedermann. This growth episode may coincide with St. Germain I-C; hence, it could correlate with the Brørup episode of the δ^{18}O record of GRIP (Dansgard *et al.,* 1993). As the faunal record of this deposit is not well constrained, a direct comparison with the Grand Pile peat bog is not yet possible.

The peat and ice core records, both representing Northern Hemisphere climate variations, likely reflect climate change that forced travertine formation and thus should agree with the travertine growth history. However, because of uncertainties in the dating of the ice and peat, these correlations are speculative.

The travertine history can also be compared with the SPEC-MAP curve and with Northern Hemisphere insolation variations (Fig. 7C). The major growth episodes during substage 5.3 coincide with a peak of Northern Hemisphere insolation, suggesting the possible correlation of carbonate precipitation and warm climate. However, neither the insolation record nor the SPECMAP record resolves the cooling event that is represented by the silt layer and by the ice core and peat records.

CONCLUSIONS

Thermal spring deposits at two sites near Stuttgart grew with high accumulation rates of up to 5 mm yr^{-1}. The resulting travertine records are most likely discontinuous and correspond only to short periods of a few hundred to a few thousand years. The two sites differ in groundwater chemistry (U/Sr and initial ^{234}U/^{238}U ratio).

Growth episodes are restricted to the end of substage 5.5, with a high accumulation period during substage 5.3. They likely correspond to climatic changes recorded by the peat bog pollen records from Grand Pile and Les Echets and by δ^{18}O values of the GRIP ice core.

We found no evidence of travertine formation during substages 5.1 and 3, in agreement with the lack of secondary carbonate growth during these intervals in northern Europe reported by Baker *et al.* (1993). Such lack of evidence of
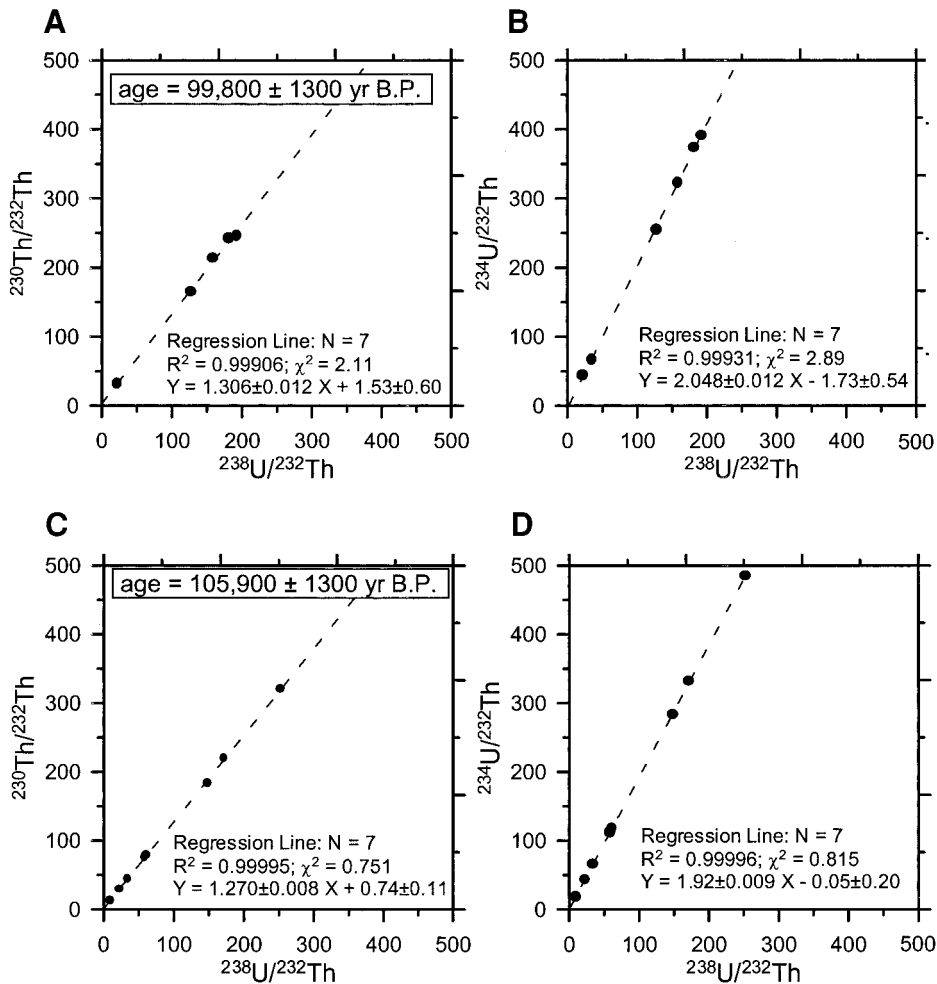
FIG. 6. Rosholt type II isochrons for laminar travertine samples of Deckerstrasse (A, B) and Biedermann (C–D) deposits. Plotted are the activity ratios of $^{230}Th/^{232}Th$, $^{234}U/^{232}Th$, and $^{238}U/^{232}Th$. The applied error weighted linear regressions yield R^2 values of >0.9995 and $\chi^2 \sim 0.5$–2.5.

travertine formation near Stuttgart can be explained by lower annual precipitation, temperature, and CO_2 input from root respiration, all of which would decrease groundwater formation, HCO_3 saturation, and the consequent potential for carbonate precipitation. In addition, travertines grew close to the Neckar River; thus, presumably smaller and less-extended travertine deposits from growth episodes from substages 5.1 and 3 may have grown only close to the Neckar River, where they were subject to erosion during the succeeding glaciations.

APPENDIX

To estimate detrital contamination, we assume that the $^{230}Th/^{232}Th$ activity ratio of the spring water is representative of the ancient spring water. The spring water $^{230}Th/^{232}Th$ activity ratio can then be used to correct for contamination with initial ^{230}Th using Eq. (A1).

$$^{230}Th_a = {}^{230}Th - {}^{232}Th \cdot (R_0 - R_d) \cdot \exp(-\lambda_{230} \cdot t) - {}^{232}Th \cdot R_d \quad (A1)$$

R_0 in this model is equal to the $^{230}Th/^{232}Th$ activity ratio of present-day

spring water, R_d represents the $^{230}Th/^{232}Th$ activity ratio of detritus, $^{230}Th_a$ reflects the authigenic thorium activity derived from the decay of ^{234}U, and t is the true age of the travertine sample.

The detrital components (i.e., R_d) present in the water (high particle loads, up to 10 g liter^{-1}) can be estimated as near or below the upper continental crust value of 0.746 given by Wedepohl (1995). Considering the range of $^{230}Th/^{232}Th$ activity ratios of different rocks, a reasonable value of R_d is 0.5–0.6. To obtain a realistic estimate of the detrital fraction, we measured the radionuclide abundance of leached calcareous sands with a high detrital content ($\sim$32%). Such sands are present in all samples, because detritus is often accompanied by eroded limestone particles carried in the spring water. Iron and manganese are enriched by a factor of 4 compared to travertine samples, and the density is only 1.5 g cm^{-3}. The $^{230}Th/^{232}Th$ ($= R_d$), $^{234}U/^{232}Th$, and $^{238}U/^{232}Th$ activity ratios of 0.526 $\pm$ 0.012, 0.386 $\pm$ 0.0064, and 0.292 $\pm$ 0.004, respectively, were measured. This sample was obtained from a nearby travertine site "Haas/Lauster" (Fig. 1) ($>$200,000 yr); therefore, initial the ^{230}Th is presumably negligible. The uranium concentration is low ($^{238}U = 0.016$ ppm), indicating strong weathering of the particles. However, the uranium isotopes are not in radioactive equilibrium ($^{234}U/^{238}U = 1.32$); nor do they show a preferential leaching of ^{234}U. This is likely a result of uranium exchange processes during particle transport in spring water.
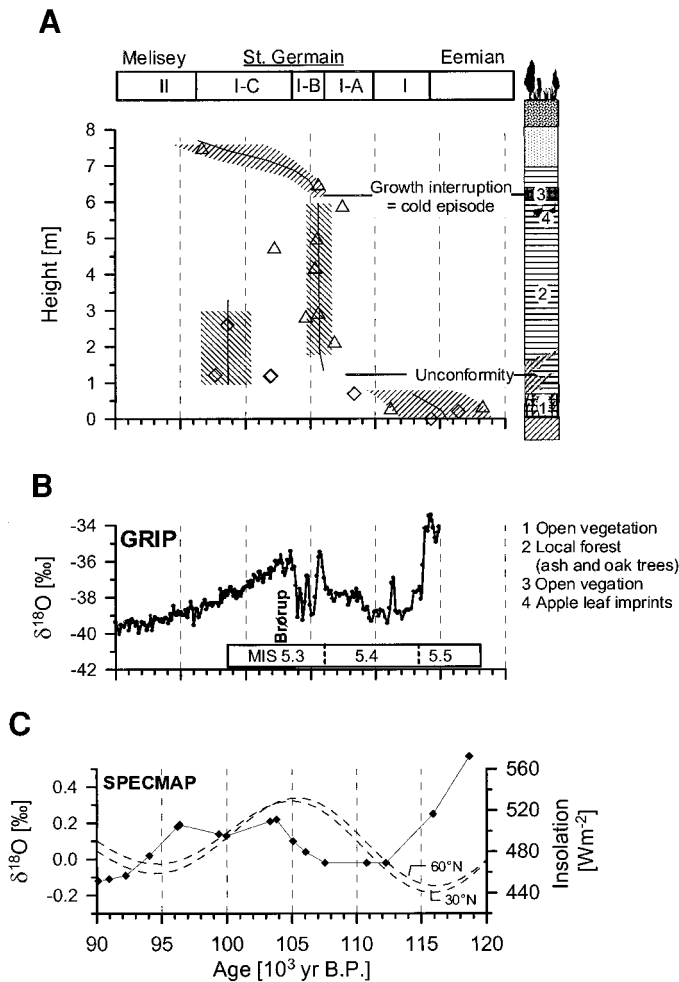
FIG. 7. Comparison of travertine growth episodes near Stuttgart (A) with other climate proxies. In part A, diagonally ruled areas and black lines represent a schematic model of travertine accumulation, derived from single ^{232}Th corrected (triangles, Biedermann; diamonds, Deckerstrasse) and ^{230}Th/U isochron ages (diagonally ruled boxes). The column on the right shows the stratigraphy of the Biedermann site. Part B shows the δ^{18}O record of the GRIP ice core (Dansgard *et al.,* 1989), and part C shows the SPECMAP curve (Martinson *et al.,* 1987) and insolation variations for 60° and 30°N (Berger and Loutre, 1991). The bar above A shows the chronology for pollen data from the Grand Pile peat bog.

The measured activity ratios of this material, together with the activity ratios of spring water, were applied to correct for detrital contamination following Eq. (A1). The correction has a statistical uncertainty of ~0.5%. Single ^{230}Th/^{234}U ages were calculated with this correction model.

to developing the cleaning procedure, and Christopher Strobl for trace metal analysis.

REFERENCES

Bard, E., Hamelin, B., Arnold, M., Montaggioni, L., Cabioch, G., Faure, G., and Rougerie, F. (1996). Sea level record from Tahiti corals and the timing of deglacial meltwater discharge. *Nature* **382,** 241–244.

Baker, A., Smart, P. L., and Ford, D. C. (1993). Northwest european palaeoclimate as indicated by growth frequency variation of secondary calcite deposits. *Palaeogeography, Paleoclimatology, Palaeoecology* **100,** 291–301.

Berger, A. L., and Loutre, M. F. (1991). Insolation values for climate for the last 10 million years. *Quaternary Science Reviews* **10,** 297–317.

Bollhöfer, A., Eisenhauer, A., Frank, N., Pech, D., and Mangini, A. (1996). Thorium and uranium isotopes in a manganese nodule from the Peru basin determined by alpha spectrometry and thermal ionization mass spectrometry (TIMS): Are manganese supply and growth related to climate? *Geol. Rundsch.* **85,** 577–585.

Braun, M., Frank, N., Goppelsröder, A., Kind, C.-J., Mangini, A., Müller, K. P., Niederhoefer, H.-J., Wagner, G., and Ziegler, R. (1998) "Deckerstrasse"—Eine mittelpaläolitische Travertin-Fundstelle in Stuttgart-Bad Cannstatt. *Fundberichte Baden-Württembergs* **22**(1), 13–44.

Burns, S., Matter, A., Frank, N., and Mangini, A. (1998). Speleothem-based paleoclimate record from Northern Oman. *Geology* **26,** 499–502.

Chen, J. H., Edwards, R. L., and Wasserburg, G. J. (1986). ^{238}U, ^{234}U, and ^{232}Th in seawater. *Earth and Planetary Science Letters* **80,** 241–251.

Dansgard, W., Johnson, S. J., Clausen, H. B., Dahl-Jensen, D., Gundestrup, N. S., Hammer, C. U., Hvidberg, C. S., Steffensen, J. P., Sveinbjörnsdottir, A. E., Jouzel, J., and Bond, G. (1993). Evidence for general instability of past climate from 250-kyr ice-core record. *Nature* **364,** 218–220.

Edwards, R. L., Chen, J. H., Ku, T. L., and Wasserburg, G. J. (1987). Precise timing of the last interglacial period from mass spectrometric determination of Th-230 in corals. *Science* **236,** 1547–1553.

Edwards, R. L., Warren Beck, J., Burr, G. S., Donahue, D. J., Chappell, J. M. A., Bloom, A. L., Druffel, E. R. M., and Taylor, F. W. (1993). A large drop in atmospheric ^{14}C/^{12}C and reduced melting in the Younger Dryas, documented with ^{230}Th ages of corals. *Science* **260,** 962–967.

Eisenhauer, A., Zhu, Z. R., Collins, L. B., and Eichstädter, R. (1996). The last interglacial sea level change: New evidence from the Abrolhos islands, West Australia. *Geol. Rundsch.* **85,** 606–614.

Ford, T. D., and Pedley, H. M. (1996). A review of tufa and travertine deposits of the world. *Earth-Science Reviews* **41,** 117–175.

Goudie, A. S., Viles, H. A., and Pentecost, A. (1993). The late Holocene tufa decline in Europe. *The Holocene* **3,** 181–186.

Grün, R., Brunnacker, K., and Hennig, G. J. (1982). ^{230}Th/^{234}U-Daten mittel- und jungpleistozäner Travertine im Raum Stuttgart. *Jber. Mitt. Oberrhein. Geol. Ver.* **64,** 201–211.

Guiot, J., Pons, A., de Beaulieu, J. L., and Reille, M. (1989). A 140,000-year continental climate reconstruction from the two European pollen records. *Nature* **338,** 309–313.

Harmon, R. S., Schwarcz, H. P., and O'Neil, J. R. (1979). D/H ratios in speleothem fluid inclusions: A guide to variations in the isotopic composition of meteoric precipitation? *Earth and Planetary Science Letters* **42,** 254–266.

Ivanovich, M., and Harmon, R. S. (1992). "Uranium Series disequilibrium: Applications of Earth, Marine, and Environmental Science." Clarendon, Oxford.

Kaufman, A. (1992). An evaluation of several methods for determining ^{230}Th/U ages in impure carbonates. *Geochimica et Cosmochimica Acta* **57,** 2303–2317.

Kaufman, A., and Broecker, W. (1965). Comparison of ^{230}Th and ^{14}C Ages for carbonate materials from Lakes Lahotan and Bonneville. *Journal of Geophysical Research* **70,** 4039–4054.

Koban, C. G. (1993). Faziesanalyse und Genese der quartären Sauerwasserkalke von Stuttgart, Baden Württemberg. *Profil* **5,** 47–118.

Lin, J. C., Broecker, W. S., Anderson, R. F., Hemming, S., Rubenstone, J. L., and Bonani, G. (1996). New ^{230}Th/U and ^{14}C ages from Lake Lahotan carbonates, Nevada, USA, and a discussion of the origin of initial thorium. *Geochimica et Cosmochimica Acta* **60,** 2817–2832.

Ludwig, K. R., Simmons, K. R., Szabo, B. S., Winograd, L. J., Landwehr, J. M., Riggs, A. C., and Hoffman, R. J. (1992). Mass spectrometric ^{230}Th-^{234}U-^{238}U dating of the Devils Hole Calcite Vein. *Science* **258,** 284–287.

Ludwig, K. R., and Titterington, D. M. (1994). Calculation of ^{230}Th/U isochrons, ages and errors. *Geochimica et Cosmochimica Acta* **58,** 5031–5042.

Martinson, D. G., Pisias, N. G., Hays, J. D., Imbrie, J., Moore, T. C., and Shackelton, J. N. (1987). Age dating and the orbital theory of the Ice Ages: Development of a high-resolution 0 to 300,000 year chronostratigraphy. *Quaternary Research* **27,** 1–29.

McDermott, F., Grün, R., Stringer, C. B., and Hawkesworth, C. J. (1993). Mass-spectrometric U-series dates for Israeli Neanderthal/early modern hominid sites. *Nature* **363,** 252–255.

Pedley, M. H. (1994). Prokaryote-microphyte biofilms and tufas: A sedimentation perspective. *Darmstädter Beiträge zur Naturgeschichte* **4,** 45–60.

Pentecost, A. (1996). The Quaternary travertine deposits of Europe and Asia Minor. *Quaternary Science Reviews* **14,** 1005–1027.

Reiff, W. (1986). Die Sauerwasserkalke von Stuttgart. *Fundberichte aus Baden Württemberg* **11,** 2–24.

Reille, M., and de Beaulieu, J. L. (1990). Pollen analysis of a long upper Pleistocene continental sequence in a Velay maar (Massif Central, France). *Palaeogeography, Palaeoclimatology, Palaeoecology* **80,** 35–48.

Roberts, M. S., Smart, P. L., and Baker, A. (1998). Annual trace element variation in a Holocene speleothem. *Earth and Planetary Science Letters* **154,** 237–246.

Schweigert, G. (1991). Die Flora der Eem-interglazialen Travertine von Stuttgart-Untertuerkheim (Baden-Wuerttemberg). *Stuttgarter Beitraege zur Naturkunde, Serie B* **178,** 1–43.

Sturchio, N. P., Pierce, K. L., Murrel, M. T., and Sorey, M. L. (1994). Uranium-series ages of travertines and timing of the Last Glaciation in the northern Yellostone Area, Wyoming–Montana. *Quaternary Research* **41,** 265–277.

Taylor, D. M., Griffiths, H. I., Pedley, H. M., and Prince, I. (1994). Radiocarbon-dated Holocene pollen and ostracod sequence from barrage tufa-dammend fluvial systems in the White Peak, Derbyshire, UK. *The Holocene* **4,** 356–364.

Ufrecht, W. (1994). Das Mineral- und Heilwasser von Stuttgart-Bad Cannstatt und Berg-eine Einfuehrung in die Geologie, Geohydraulik und Hydrochemie des Systems. *In* "Das Mineral-und Heilwasser von Stuttgart" (W. Ufrecht and G. Einsele, Eds.), pp. 13–48. Schriftenreihe des Amtes für Umweltschutz, Stuttgart.

Wedepohl, K. H. (1995). The composition of the continental crust. *Geochimica et Cosmochimica Acta* **59,** 1217–1232.

Woillard, G. M. (1976). Grande Pile Peat Bog: A continuous pollen record for the last 140,000 years. *Quaternary Research* **9,** 1–21.